Article

Structural and Geochemical Assessment of the Coralline Alga *Tethysphytum antarcticum* from Terra Nova Bay, Ross Sea, Antarctica

Matthias López Correa [1,2], Sebastian Teichert [1], Federica Ragazzola [3,*], Salvador Cazorla Vázquez [4], Felix B. Engel [4], Katrin Hurle [1], Claudio Mazzoli [5], Piotr Kuklinski [6], Giancarlo Raiteri [7] and Chiara Lombardi [7]

1 GeoZentrum Nordbayern, Friedrich-Alexander-Universität Erlangen-Nürnberg, 91054 Erlangen, Germany
2 Consiglio Nazionale delle Ricerche, Istituto di Scienze Marine, Via Gobetti 101, 40129 Bologna, Italy
3 Department of Integrative Marine Ecology, Ischia Marine Centre, Stazione Zoologica Anton Dohrn, Punta San Pietro, Ischia, 80077 Naples, Italy
4 Experimental Renal and Cardiovascular Research, Department of Nephropathology, Institute of Pathology, Friedrich-Alexander-Universität Erlangen-Nürnberg, 91054 Erlangen, Germany
5 Department of Geosciences, University of Padova, 35131 Padova, Italy
6 Department of Marine Ecology, Institute of Oceanology, Polish Academy of Sciences, 81-712 Sopot, Poland
7 Marine Environment Research Centre of S. Teresa, ENEA (Italian National Agency for New Technologies, Energy and Sustainable Economic Development), 19032 Lerici, Italy
* Correspondence: federica.ragazzola@szn.it

Abstract: Crustose coralline algae (CCA) occur from the tropics to the poles in photic benthic environments. Here, we report on some of the world's southernmost and coldest CCA sites in Terra Nova, Ross Sea, Antarctica at 74°41′ S. The recently described red alga *Tethysphytum antarticum* is investigated for its skeletal architecture, its mineralogical and geochemical composition, as well as for its taxonomic classification. A phylogenetic analysis based on molecular genetics and the sequencing of the photosystem II protein D1 (psbA) gave a perfect match with *T. antarticum*. Histological sections and micro-CT-scans provide new diagnostic details for the conceptacles (the reproductive organs of the alga). X-ray diffractometry and electron-microprobe measurements yielded a clear high-Mg calcite (~8 mol%) composition of the skeletal parts. Detailed back-scattered electron imaging of polished petrographic thin sections revealed a two-layered thallus (vegetative plant tissue), comprising an organic-rich irregularly calcified basal layer with rectangular cells, overlain by the main thallus. Elemental maps show relatively increased sulphur in the basal layer, clearly tied to organic cell walls. $MgCO_3$ and $SrCO_3$ were targeted with semiquantitative elemental mappings and in an ontogenetic quantitative spot transect. Compared with temperature (−1.95 °C to +1.08 °C), the $MgCO_3$ (mol%) reflects this world's coldest CCA site temperature with the lowest $MgCO_3$ content of 7.9 ± 1.6 mol%. The along transect variability, however, shows with ~6 mol% a larger $MgCO_3$ variability than expected for the 3 °C intra-annual temperature amplitude in Terra Nova Bay. This implies that in low amplitude settings the biomineralisation control on Mg/Ca ratios can outcompete its temperature sensitivity. Mark-recapture studies, next to the environmental logger station La Zecca are suggested, to perform a detailed growth rate and biomineralisation quantification.

Keywords: crustose coralline algae; Antarctica; taxonomy; phylogeny; thallus structure; biomineralization; geochemistry; climate change

1. Introduction

Crustose coralline algae (CCA) represent a major component of most benthic ecosystems from the poles to the tropics. They providing ecosystem services and comprise up to half of the carbonate-secreting organisms in some cold water habitats [1]. CCA are

important habitat builders and increase benthic diversity by providing hard substrate for other organisms to settle on [2,3].

Their thallus is composed of high-Mg calcite, the most soluble form of $CaCO_3$, with calcification occurring in the cell wall guided by a polysaccharide matrix [4,5]. Mg content in the thallus is driven by the endothermic substitution of Mg in calcite, favoring the Mg substitution at higher temperatures [6]. Following this principle, Mg/Ca ratios in CCAs have been used for temperature reconstruction in long living and subfossil marine species [6,7]. It has been estimated that the Mg content in CCA varies between 7.7 to 28.8 $MgCO_3$ (mol%) [8] depending on the region they live in [9,10]. Due to the higher solubility of high-Mg calcite, the calcified thallus of CCA is more vulnerable to ocean acidification especially in cold water environments such as polar regions where the water naturally has a lower saturation state, and higher solubility of CO_2.

CCAs have been described as being widespread in the Ross Sea [11] both in shallow and deep environments [12], often forming a large component of the understory beneath stands of canopy-forming algae [13] of CCA to dominate the flora at high-latitude marine systems. There, sea-ice cover plays a major role in modulating the seasonal seafloor illumination, which is directly relevant to the photosynthetic efficiency of CCAs [14].

Even though CCA cover a wide proportion of bedrock substrates, collections made in recent decades in the Ross Sea suggest to be a species poor environment for CCAs [15]. However, the lack of diversity was probably the result of sampling constraints and a species-level assessment based only on morpho-anatomical characters. CCA surveys in Terra Nova Bay (Ross Sea) in recent decades reported the presence of three species, *Leptophytum foecundum* (Kjellman) W.H. Adey [16], *Clathromorphum lemoineanum* Mendoza & Cabioch, 1985 [12,17,18] and *Tethysphytum antarcticum* Sciuto, Moschin & Moro 2021 [19]. In the next decades, the diversity and knowledge of CCA in Antarctica will most likely expand with the use of molecular-assisted taxonomy, which already has revolutionized our understanding of coralline diversity and phylogenic relationships [20,21].

The studies on species diversity should also include information on thallus composition. Especially for high-Mg calcite calcifiers, it is important to provide a baseline for understanding organismal vulnerability to the future impacts of ocean acidification.

While for some taxa the collection of this information is already underway [22], so far very little information is present for CCAs. The aim of this study is to start filling the gap of our knowledge on CCAs skeletal composition in Antarctica.

2. Materials and Methods

2.1. Study Site Characteristics and Sample Collection

The study site—Terra Nova Bay (TNB)—is located at the southwestern edge of the Ross Sea, representing the center of the highest productivity of the Southern Ocean (SO) [23,24]. Global biogeochemical cycles and the sequestration of anthropogenic CO_2 into the deep ocean [25] are mainly driven by the SO, thus all alterations driven by climate change are consequently impacting its ecosystems with potentially large effects on coastal environments. Such changes include increased temperature and altered sea ice coverage, iceberg scouring of benthic habitats, ocean acidification, salinity/freshening, and low oxygen levels [26–28].

With an extension of approximately 80 km × 30 km, a mean depth of about 450 m, with greater depths close to the coast and up to 1000 m depths in the near basin, TNB is delimited by the narrow peninsula of Cape Washington (74°44′ S 163°45′ E), at the north side, and by the Drygalski Ice Tongue (64°43′ S 60°44′ W), at the south side. The orography of the region determines TNB climate by driving atmospheric fluxes, which creates dynamic systems such as barriers and katabatic winds. These winds are keeping the area free of ice, causing temperature drops (surface seawater temperature range: −1.9, +1 °C) [29] and a delay in summer seawater stratification. Furthermore, they are also responsible for formation and maintenance of polynyas (i.e., persistent and recurrent regions of open water and with thin ice or reduced ice concentration) persisting during wintertime [30], that, in

coastal areas, are generated by persistent wind driven export of sea ice causing continuous sea ice formation, with consequent strong heat loss and salt injection [31].

Sea ice coverage, occurring for at least 9 months a year [32], as well as current and water mixing [33], are affecting changes in species composition at the study site, but also physiological processes of benthic ecosystems (i.e., photosynthesis, respiration, calcification). The variability of the surface carbonate system properties at the study site has been observed to be primarily controlled by biological activity [23,34]. During summer months when the ice melts, phytoplankton blooms greatly affect the carbonate system [32]. Furthermore, the local productivity of benthic ecosystems is primarily characterized by calcifying organisms [35,36]. These comprise CCA, bryozoa, corals, sponges, mollusks and echinoderms. The intensification of calcifiers' physiological activities, such as photosynthesis, feeding and reproduction for filter feeders, and calcification (i.e., growth of their calcified thalli and skeletal structures) [37,38] affect dissolved oxygen, $p\mathrm{CO_2}$, and saturation state reduction observed in the site during summer [23].

Specimens of *Tethysphytum antarcticum* in the shape of thin, cobble-coating coralline algal crusts have been collected during XXXIV Italian Expedition to Antarctica (November 2018) in Tethys Bay by means of Scuba diving, at Site 1 (coordinates: 74°41.402′ S, 164°06.344′ E), at 24 m water depth. Collected samples were placed in thermic boxes, transported to the laboratory at "Mario Zucchelli Station", dried in desiccation chambers, and stored in plastic bags (LD-PE) together with silica gel as a drying agent.

2.2. Species Identification

2.2.1. Morphological Investigations

Macroscopic overview images of nine specimens were photographed using a Zeiss 50 mm macro lens mounted on a Nikon D750 DSLR (Malaysia). One specimen (Ross-07) was chosen for the further examinations in this study and additionally photographed with a Zeiss Axio Zoom.V16 (Germany), equipped with a Zeiss Plan-NEOFLUAR Z $1\times/0.25$ FWD 56 mm (Germany). The software Zeiss ZEN core 2.7.0 (Germany) was used to produce high-resolution images via the tile stitching mode and an EDF motorized focus (6 z-slices per tile). All images were post-processed in Adobe Photoshop by means of sharpening, tonal value adjustment, and shadows/highlights adjustments.

To visualize how the crusts of *T. antarcticum* are attached to their substrate, one specimen (Ross-7) was prepared for X-ray micro-computed tomography (μCT). One cobble covered by an algal thallus (Figure 1) was sampled by a water-cooled, hollow diamond drill bit with an inner diameter of 10 mm. The drill bit was mounted on a Fein ASCM 18 QM electric drill operated in a Fein drill rig. The resulting drill core was mounted to a borosilicate glass rod using hot-melt adhesive.
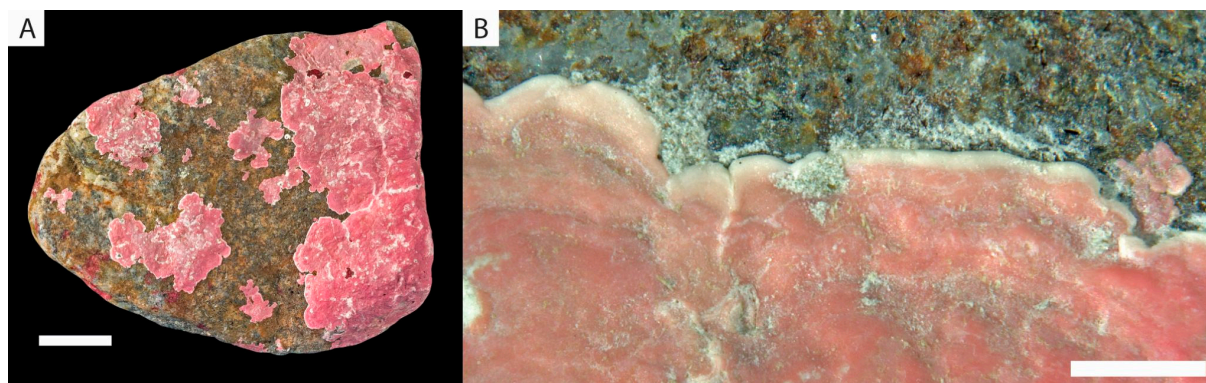

Figure 1. Overview of specimen Ross-7 with several individuals of *T. antarcticum* (**A**) and detail of the growing margins of two individuals (**B**). Scale bars = 1 cm.

The scan was performed on a General Electric Phoenix v│tome│x s 240 μCT scanner (Wunstdorf, Germany) with a GE x-ray source xs│240d with a tungsten target and a GE flat panel detector DXR250RT with 1000 × 1000 pixels, using a 0.1 mm copper filter. During a full rotation of each sample, 1500 frames were taken at 200 ms exposure time at 100 kV and 100 mA of current, resulting in a scanning time of 40 minutes. Raw data were reconstructed with GE datos│x software version 2.4, using a Feldkamp algorithm based on filtered back projection. For noise reduction of the reconstructed data set, a median filter (VolumeGraphics Studio MAX software version 3.0, Heidelberg, Germany) within a local neighborhood of 3 voxels (diameter of neighborhood area) was used. All post-processing was performed with the VolumeGraphics software.

Samples for scanning electron microscopy (SEM) were prepared from the drill core produced for the μCT analysis and another part of specimen Ross-07 that had been cut off by a Steinadler low-speed, water-cooled diamond saw. The samples were mounted on aluminum stubs using PONAL express wood glue and sputter coated with gold under argon in a Cressington 108 auto for 6 min (3 × 2 min intervals) at 30 mA and 10,000 V. SEM-micrographs were taken with a Tescan Vega\\xmu (Prague, Czech Republic) at 20 kV in secondary electron mode. SEM images were post-processed in Adobe Photoshop by means of sharpening, tonal value adjustment, and shadows/highlights adjustments.

Complementary to the SEM investigations, a further sample slice was cut perpendicular to the rock and algal crust, to examine the skeletal mineralogy and crystal orientation.

In an EPOVAC chamber, the dry sample was vacuum-embedded in a two-component epoxy resin (Biresin L48 resin and hardener, 4:1), cured 48 hours, cut with a water-cooled PRESI Mecatome precision rock saw and grinded on a PRESI Minitech 300 SPI using diamond discs with 125 μm, 75 μm, 54 μm, and 18 μm graining. The surface was then glued with BIRESIN epoxy resin to a glass slide and ground to 20 μm final thickness using a G&N MPS 2 R300 (Germany). Sections were photographed in normal and polarized translucent light with a Zeiss Axio Zoom.V16 (Germany), equipped with a Zeiss Plan-NEOFLUAR Z 1×/0.25 FWD 56 mm (Germany). The software Zeiss ZEN core 2.7.0 (Germany) was used to produce high-resolution images via the tile stitching mode. All images were post-processed in Adobe Photoshop by means of sharpening, tonal value adjustment, and shadows/highlights adjustments.

Pieces of the Ross-7 specimen were fixated at room temperature for seven days in a 10% formalin-bearing seawater solution. Decalcification was performed for 24 h at room temperature with 0.6N HNO_3. The remaining algal soft tissue sheets were then manually detached from the boulder surface with a scalpel under a microscope. Post-fixation with 10% formalin was followed by a dehydration step and a xylol-paraffin transition.

The oriented samples were embedded In Paraffin, cut with a LEICA microtome into 4 μm thick slices for phase contrast microscopy screening and were then rehydrated. Histological sections were preferentially placed at the rare sites with conceptacles on the crust surface, to complement the taxonomic assessment. High resolution images were captured on a Zeiss LSM800 confocal laser scanning microscope (Germany) operated with the software Zeiss ZEN core 2.7.0 and using an EDF motorized focus (10 z-slices per image). All images were post-processed in Adobe Photoshop by means of sharpening, tonal value adjustment, and shadows/highlights adjustments.

2.2.2. Phylogenetic Analysis

To confirm the taxonomic assignment of the Ross-7 specimen to *T. antarcticum* by molecular genetics and to further resolve the relationships within the respective clade, the photosystem II protein D1 (psbA) was sequenced using Sanger sequencing and two primer sequences:

ATG ACT GCT ACT TTA GAA AGA CG (psbA-F)
GCT AAA TCT ARW GGG AAG TTG TG (psbA-R1)

according to Yoon et al. [24]. For the taxonomic assignment, the gained psbA sequence of Ross-7 was then saved as a FASTA file and analyzed using the BLASTn tool in GenBank (https://blast.ncbi.nlm.nih.gov/Blast.cgi accessed on 30 January 2023).

For the phylogenetic reconstructions, the psbA sequences from [19] and [39,40] as well as the Ross-7 sequence were combined to a single FASTA file and loaded in the software Mega X [41]. The alignment was constructed via ClustalW, using a gap opening penalty of 15.00 and a gap extension penalty of 6.66 for the pairwise alignment and a gap opening penalty of 15.00 and a gap extension penalty of 6.66 for the multiple alignment. The DNA weight matrix was set to IUB with a transition weight of 0.50. After the aligning procedure, the final alignment was visually checked and exported to the MEGA-format.

The best nucleotide substitution model was inferred via the Bayesian Information Criterion (BIC) and the substitution pattern and rates were estimated under a General Time Reversible model with a discrete Gamma distribution to model evolutionary rate differences among sites (5 categories, parameter = 0.2794) and the rate variation model allowed for 21% of sites to be evolutionarily invariable (GTR + G + I). A maximum likelihood approach was used to estimate the Gamma parameter for site rates and a discrete Gamma distribution was used to model evolutionary rate differences among sites. For estimating the maximum likelihood values, a tree topology was automatically computed.

The phylogenetic tree was reconstructed with a maximum likelihood approach, using 1000 bootstrap replications and a General Time Reversible model with a discrete Gamma distribution with 5 rate categories and assuming that a certain fraction of the sites are evolutionarily invariable (GTR + G + I). The heuristic method for the maximum likelihood approach was a Nearest-Neighbor-Interchange (NNI).

2.3. Calcified Thallus Structure, Mineralogy and Element Characterization

For determining the main mineralogical components of the thallus, specimens were analyzed via X-ray diffraction (XRD) on carbonate powders (3 replicates). A small amount of the algal skeleton was slightly crushed with an agate mortar and prepared into a special single-crystal silicon cavity sample holder via front loading method. The XRD measurement was performed at a D8 Advance with DaVinci design diffractometer (Bruker AXS, Karlsruhe, Germany) with the following parameters: angle range 7–85° 2θ; step size 0.0112° 2θ; integration time 0.4 s per step; divergence slit 0.3°; radiation: Cu K$_\alpha$; generator settings: 40 mA, 40 kV. Rietveld refinement was conducted with software TOPAS V5 (Bruker AXS, Karlsruhe, Germany). For the refinement of calcite, the structure ICSD #80869 was applied together with a Chebychev polynomial of 8th order for the background. Refined parameters were scale factor, lattice parameters, crystallite size (Lorentz contribution) and microstrain (Gauss contribution).

For determining the elemental composition and realizing the qualitative elemental maps of the thallus, Electron Microprobe (EMP) analysis was performed. Along a 6.75 mm long transect spot measurements of elemental compositions have been acquired with an Electron-Microprobe (EMP) at the Mineralogy Institute of GZN at the University of Erlangen-Nuremberg in Germany. The JEOL Superprobe was operated at 15 kV acceleration voltage and 15 nA probe current with a focused electron beam for quantitative measurements of Sr (Lα, PETJ) S (Kα, PETH), Mg (Kα, TAP) and Ca (Kα, PETJ)—abbreviations TAP, PETH, PETJ stand for respective monochromator crystals. Dwell time was 20 s per element, with 10 s background acquisition. Data were calculated as oxides, background corrected, with CO_2 kept as stable at its theoretical content in $CaCO_3$ with 43.95% and O as O^{2-} anion. Calibrated standard materials for wave length dispersive spectra were MgO, Wollastonite, celestine and PbS for Mg, Ca, Sr and S, respectively. Targeted elements were expressed as total weight percent of their oxides MgO, CaO, SrO, SO_2 and CO_2. Owing to the porous nature of the algal thallus and the thin cell wall structures, raw yields were on average ~92% and oxide weight per cents were hence normalized to 100%. Each of the 64 spot positions were individually focused and topographic effects are hence negligible. The grand majority of spot measurements targeted the dense cell walls (n = 58), while in

several positions targeted also the stratum underlying the monomeral thallus (n = 6). All data are additionally expressed as ratios of Mg/Ca, Sr/Ca and S/Ca, with CO/Ca utilized as signal yield indicator. Results of four spot measurements #24, 27, 59 and 64 were treated as outliers, e.g., for having unrealistically low Mg-contents of <<1 weight%.

Qualitative element maps were acquired with a defocused electron beam (15 kV, 15 nA, 200 ms dwell time), with a 1×1 μm resolution. EMP maps targeted three areas across the entire thallus width including the underlying stratum. Map sizes were 500×150 μm, 450×150 μm and 200×150 μm. Elemental distributions of Mg, Sr, S, Mn and Ca are plotted as weight% normalized to the map's area, accompanied by a compound image for all acquired elements. For Mn, Rhodonite (LiF) was used as calibrated standard.

3. Results

3.1. Species Identification

According to the plant characteristics (vegetative features) visible in macroscopy, SEM microscopy as well as histological sections, we identify the individuals colonizing the Ross-7 specimen as *Tethysphytum antarcticum* Sciuto, Moschin & Moro, 2021. This assumption is strengthened by the phylogenetic analysis outlined in the next section. The crustose non-geniculate thalli that colonize cobbles of various sizes are pink in color, lack protuberances or branches, and have a relatively smooth surface (Figure 1).

The thalli are pseudoparenchymatous (i.e., algae are made of loose or close aggregation of numerous, intertwined, branched filaments that collectively form the thallus) and have a monomerous construction (i.e., a construction pattern with a single system of repeatedly branched filaments), consisting of filaments running more or less parallel to the substrate, arranged to form a ventral region or central core, and a peripheral region where these filaments changed in direction curving up towards the thallus surface (Figure 2A–D). Cells are joined by cell fusions and cell walls consist of early needle crystals running parallel to the cell wall and later needle crystals running perpendicular to the cell wall (Figure 2E–F).

The conceptacles are tetrasporangial and have multiporate plates (Figure 3A–D), implying that the content of the sporangium (the capsule structure in which the reproductive spores are produced) divides to form four spores and that the roof of the sporangium has several openings. Contrary to the observations in Sciuto et al. [19], the pore plates are not flat topped with slightly raised rims, but dome shaped (Figure 3C). The conceptacle chambers are elliptical and develop within the dorsal region (Figure 3A–B). For the alga structure see Figure S3 in the supplementary information.

The psbA-sequencing of Ross-7 resulted in 919 base pairs. BLASTn results indicated a 100% identity to both *T. antarcticum* specimens (GenBank accession numbers LR812099.1 and LR861817.1) described in Sciuto et al. [19] with 99% and 97% query coverage, respectively; therefore, allowing for a definite identification of the Ross-7 specimen as *T. antarcticum*.

The best nucleotide substitution model inferred via the Bayesian Information Criterion was a General Time Reversible model with a discrete Gamma distribution with five rate categories and assuming that a certain fraction of sites is evolutionarily invariable (GTR + G + I). The estimated value of the shape parameter for the discrete Gamma distribution was 0.2794 and the proportion of sites estimated to be invariant was 21%.

The evolutionary rate differences among sites were 0.00, 0.04, 0.23, 0.87, 3.86 substitutions per site (Table 1) with nucleotide frequencies of A = 25.63%, T/U = 33.60%, C = 20.59%, and G = 20.18%.
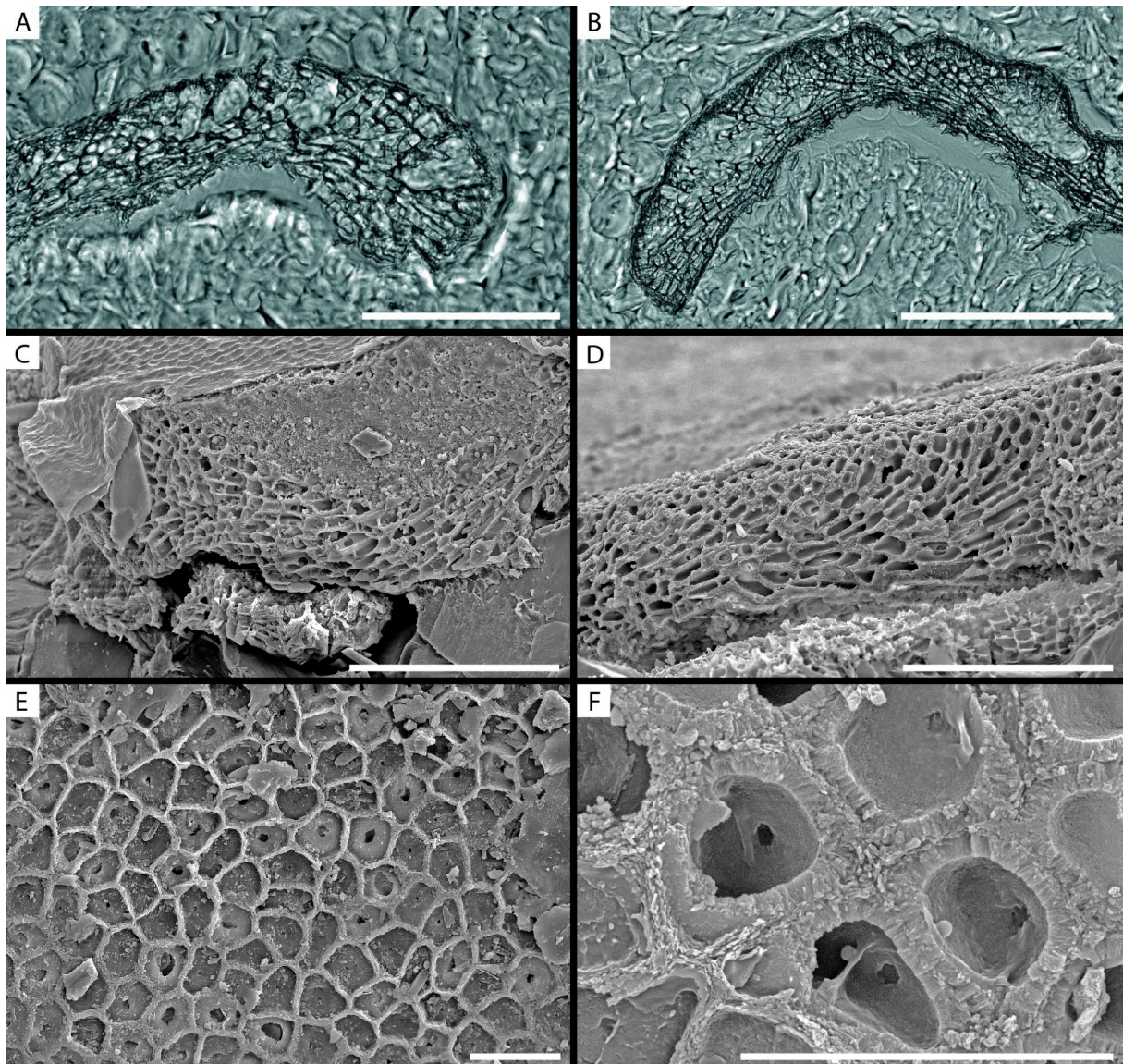
Figure 2. Vegetative features of *T. antarcticum* in histological sections (**A**,**B**) and under SEM (**C**–**F**), showing cells in the ventral thallus curving upwards (**A**–**D**), Surface layer (epithallus) (**E**,**F**) and close up of the cell wall structure showing early needle crystals running parallel to the cell wall and later formed crystal running perpendicular to the cell wall (**F**). Scale bars = 100 μm (**A**–**D**), 20 μm (**E**,**F**).

Table 1. Maximum Likelihood Estimate of Substitution Matrix.

	A	T/U	C	G
A	-	5.96	2.52	9.70
T/U	4.55	-	21.14	1.97
C	3.14	34.51	-	0.46
G	12.31	3.28	0.47	-
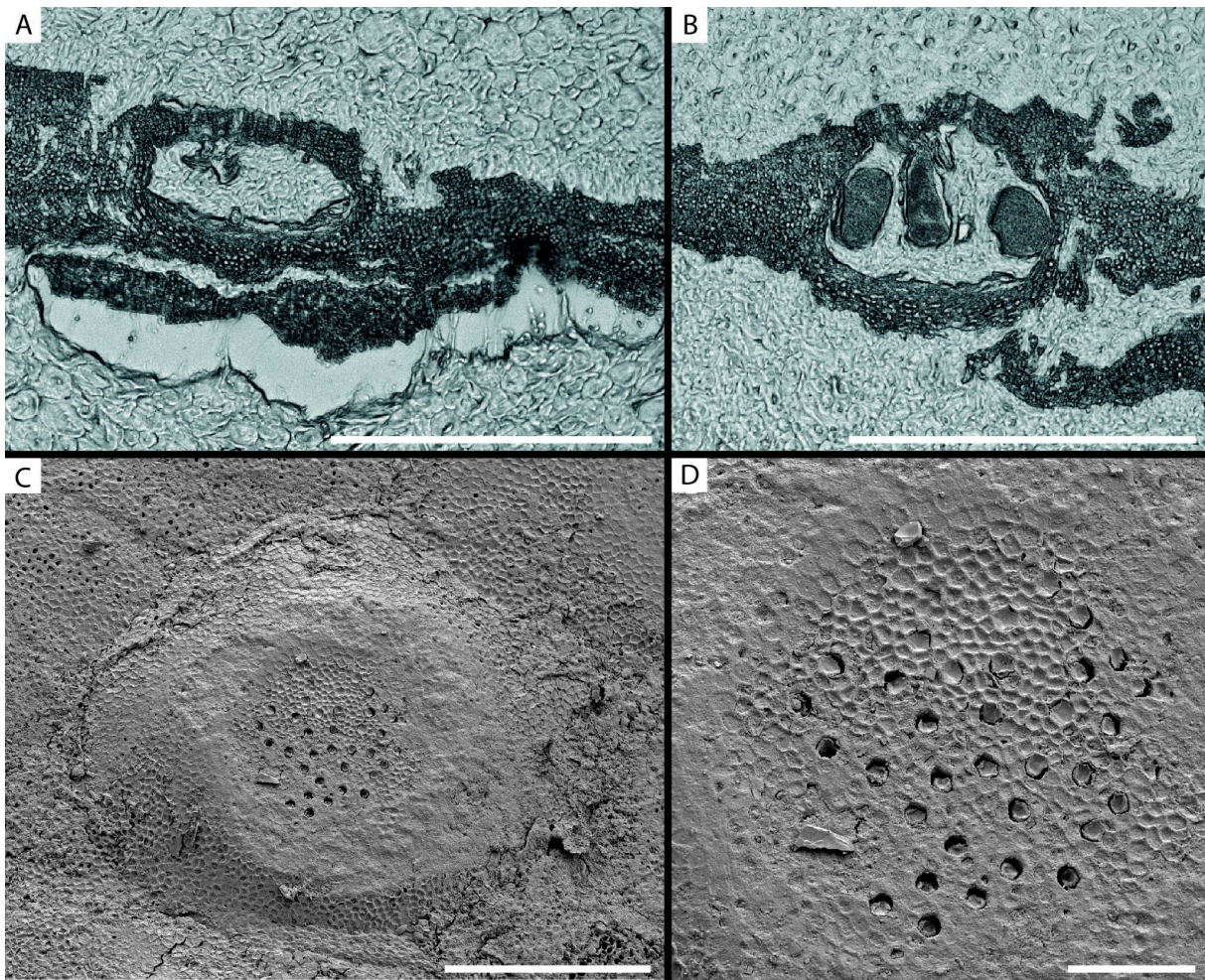
Figure 3. Vegetative features of *T. antarcticum* in histological sections (**A**,**B**) and under SEM (**C**,**D**), showing longitudinally oriented, tetrasporangial conceptacles (**A**,**B**) with surface view of the multiporate, dome shaped plates (**C**,**D**). Scale bars = 400 μm (**A**,**B**), 200 μm (**C**), 50 μm (**D**).

The evolutionary history was inferred by using the Maximum Likelihood method and a General Time Reversible model, resulting in the final tree with a log likelihood of −12018.86 (Figure 4). The tree topology corresponds to the findings of Sciuto et al. [19] and places the Ross-7 specimen in one clade with the holotype material of *T. antarcticum*. In combination with our morphological findings, we therefore identify the Ross-7 specimen as an individual of *T. antarcticum*.
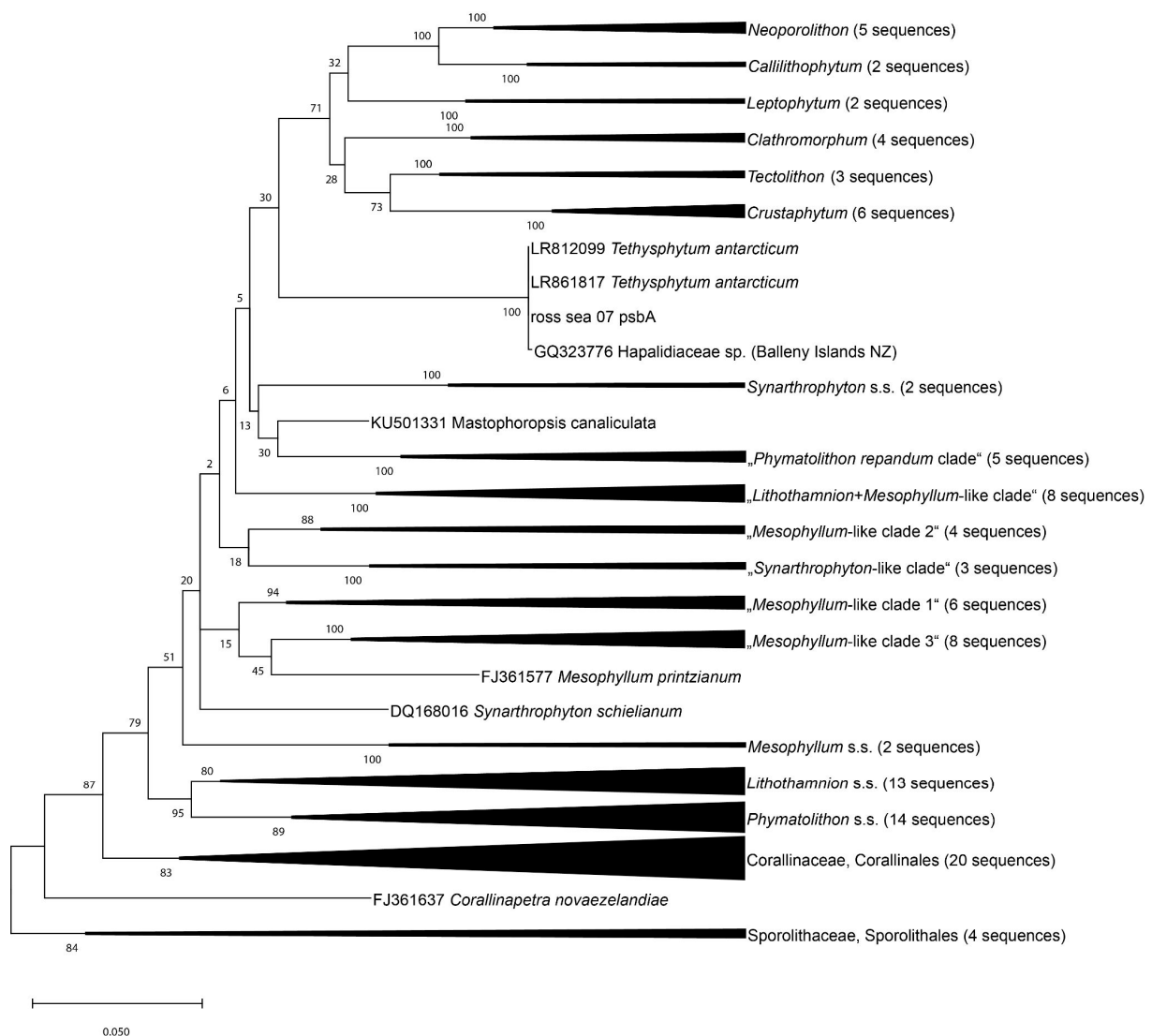
Figure 4. Final tree with a log likelihood of −12,018.86, placing the Ross-7 specimen in one clade with *T. antarcticum*. The percentage of trees in which the associated taxa clustered together is shown next to the branches. The tree is drawn to scale, with branch lengths measured in the number of substitutions per site.

3.2. Calcified Thallus Structure, Mineralogy and Elemental Composition

Our µCT analyses show that the thallus of *T. antarcticum* is rather loosely attached to its substrate, with many cavities under its dorsal site. Nevertheless, the attachment is really firm and the thallus was not easy to be remove for preparatory purposes. Reconstructed X-ray density sections (Figure 5) reveal a phaneritic hypidiomorphic texture for the substrate rock indicative of its igneous origin. The acquired Raman spectra indicated orthoclase and biotite, consistent with a granitoid compositions (spectra and methods provided in the Supplementary Materials). This rock is likely sourced from the felsic facies of the Abbott-Unit, which crops out around Tethys Bay [42]. The angular relief of this coarse crystalline substrate is covered by the monomeral thallus of the *T. antarcticum*. Interestingly, in some areas a second stratum off cells underneath the thallus, infills the uneven topography. This underlying stratum appears to contain more organic material, with conspicuous rectangular cells, that lack the characteristic wall structures of the thallus. More information on the substrate can be found in the supplementary information Figure S1.
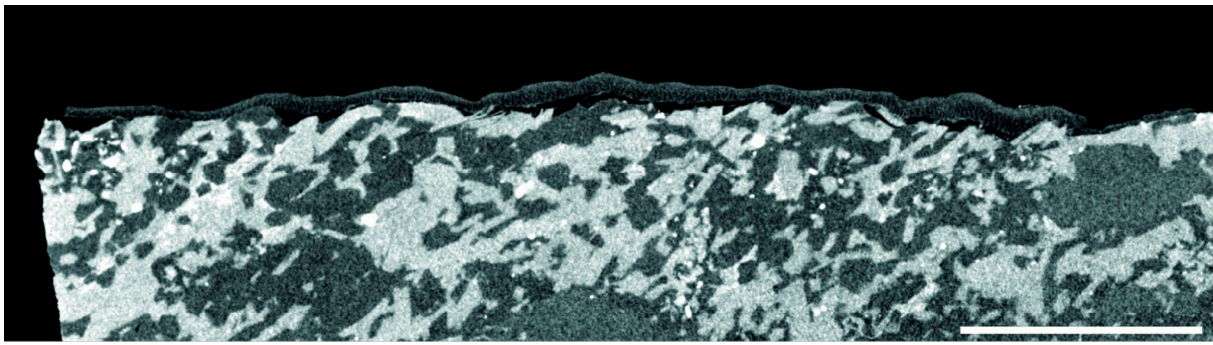
Figure 5. Reconstructed μCT image showing an attachment with an organic-rich and poorly calcified basal layer (dark), overlain by the strongly calcified main thallus (light) of *T. antarcticum* (crust thickness = ±100 μm) to its substrate. Scale bar = 1 mm.

XRD analysis revealed that calcite was the only detected carbonate phase (Figure 6). Biotite, quartz, microcline, and albite were detected in very small amounts, which is due to sample contamination from the substrate the coralline alga grew on. The sample showed a very high crystallinity and a clear microstrain was detectable. Via Rietfeld refinement, the algal skeleton contains 8.04% (±0.0007% SD) mol% $MgCO_3$, which is in line with the microprobe results (7.9 ± 1.6 mol% $MgCO_3$; Table 2). Mg content was derived via the lattice parameters using the calibrations and equations published by Titschak et al. [43] (Table S1). Since $SrCO_3$ contents are far lower than $MgCO_3$ contents (Figure 7) (by a factor of 40), we did not correct for their expectably minor influence on the lattice parameters and the $MgCO_3$ content resulting with the calibration by Titschack et al. [43]. Average lattice parameters *a* and *c* from Rietveld refinement gave 4.958 ± 0.0003 (Å) and 16.932 ± 0.0011 (Å). The unit cell volume was 360.473 ± 0.0637 (Å^3).
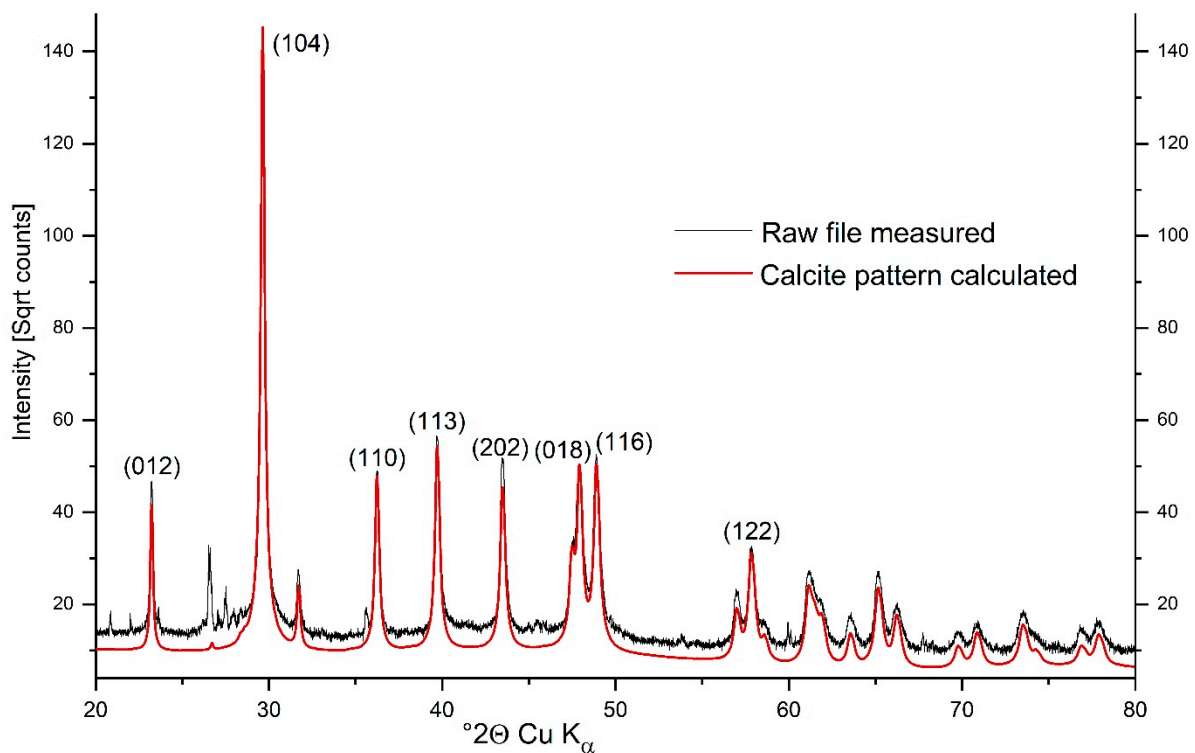

Figure 6. X-ray diffractogram with the characteristic (*hkl*)-surfaces indicated for the high-Mg calcite of the mineralized thallus.

Table 2. Summarized quantitative EMP-spot measurements of the basal thallus (n = 5) and the main thallus (n = 55).

Thallus-Unit	MgO	CaO	SrO	SO_2	CO_2	Mg/Ca	$MgCO_3$	Sr/Ca	$SrCO_3$	$CaCO_3$
	(weight%)	(weight%)	(weight%)	(weight%)	(weight%)	(mol/mol)	(mol%)	(mol/mol)	(mol%)	(mol%)
Main thallus	3.207 ± 0.642	51.809 ± 0.771	0.223 ± 0.080	0.506 ± 0.099	44.255 ± 0.121	0.086 ± 0.018	7.908 ± 1.566	0.0023 ± 0.0009	0.214 ± 0.077	91.878 ± 1.593
Basal thallus	4.787 ± 0.382	49.755 ± 0.421	0.259 ± 0.065	0.259 ± 0.065	44.384 ± 0.142	0.134 ± 0.012	11.775 ± 0.912	0.0028 ± 0.0007	0.247 ± 0.061	87.977 ± 0.948
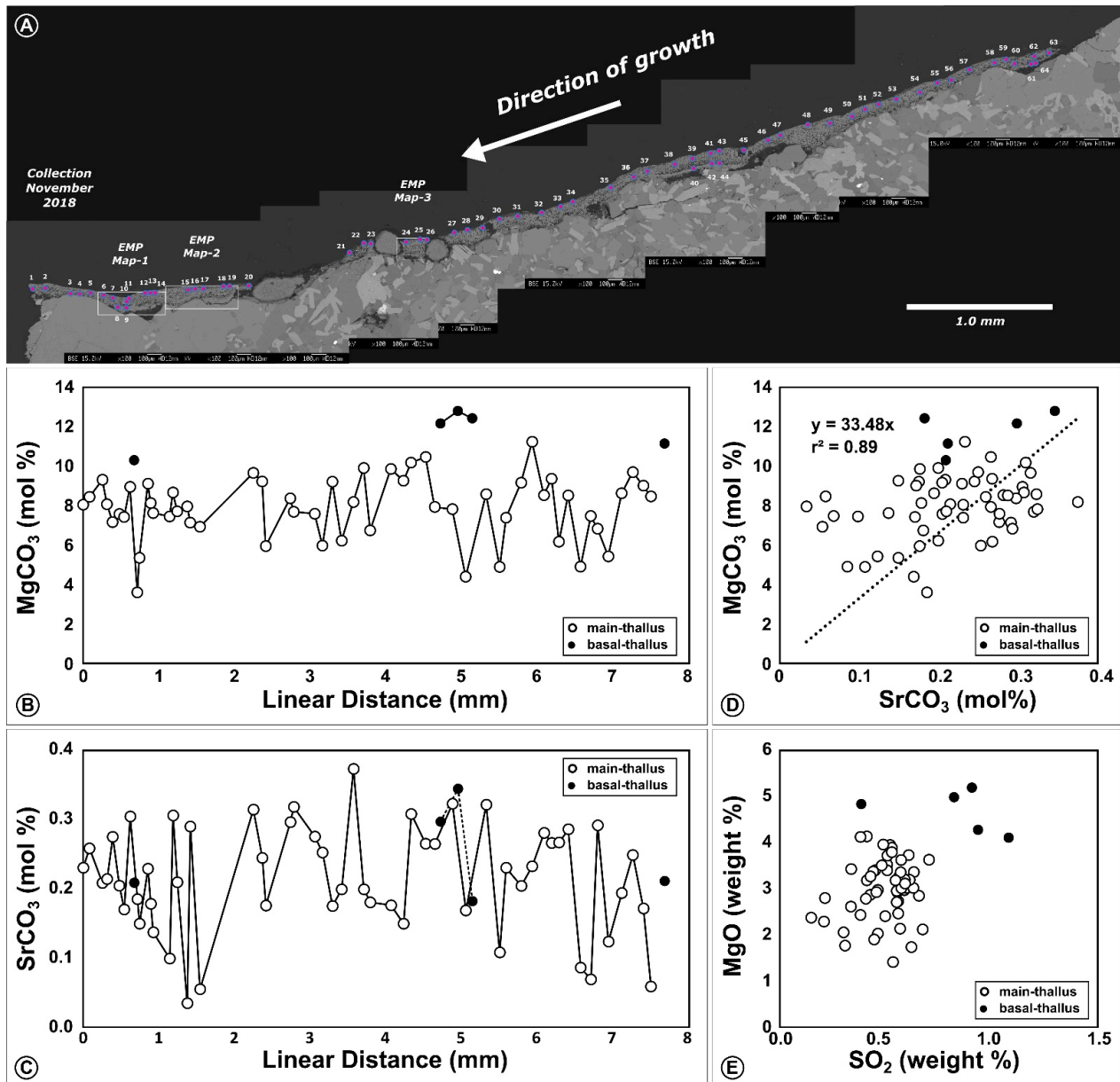
Figure 7. Overview (**A**) of the 7.5 mm long algal thallus section and the position of qualitative EMP-maps 1 to 3 and the quantitative EMP-spot measurements. Thallus growth direction is from right to left. Left margin was actively growing in November 2019. Quantitative EMP-spot measurements in the main thallus run along an ontogenetic transect from left (TNB-1) to right (TNB-64). (**B**) Quantitative EMP spot-measurements of $MgCO_3$ (mol%). (**C**) Quantitative EMP spot-measurements of $SrCO_3$ (mol%). (**D**) Relation of $MgCO_3$ (mol%) and $SrCO_3$ (mol%) from quantitative EMP spot-measurements. (**E**) Relation of MgO (weight%) and SO_2 (weight%) from quantitative EMP spot-measurements.

A representative diffractogram indicating the (*hkl*)-indices of the major calcite peaks is shown in Figure 6; the underlying spectra are provided in Figure S2.

The quantitative EMP spot measurements follow a 7.5 mm long ontogenetic transect, that crosses five conceptacles, i.e., spore-bearing chambers within the algal tissue (Figure 7). Elemental data with MgO, SrO, SO_2 and CaO (weight%), as well as Mg/Ca and Sr/Ca (mol/mol), and $MgCO_3$ and $SrCO_3$ (mol%) are summarized in Table 2. The full dataset is provided in Table S2 (supplementary material). BSE-images show a clear separation into a basal layer and a main thallus layer above, which had distinct elemental compositions (Figures 8 and 9). The ontogenetic $MgCO_3$ and $SrCO_3$ transects in the main thallus layer do not show a clear cyclicity (Figure 7).
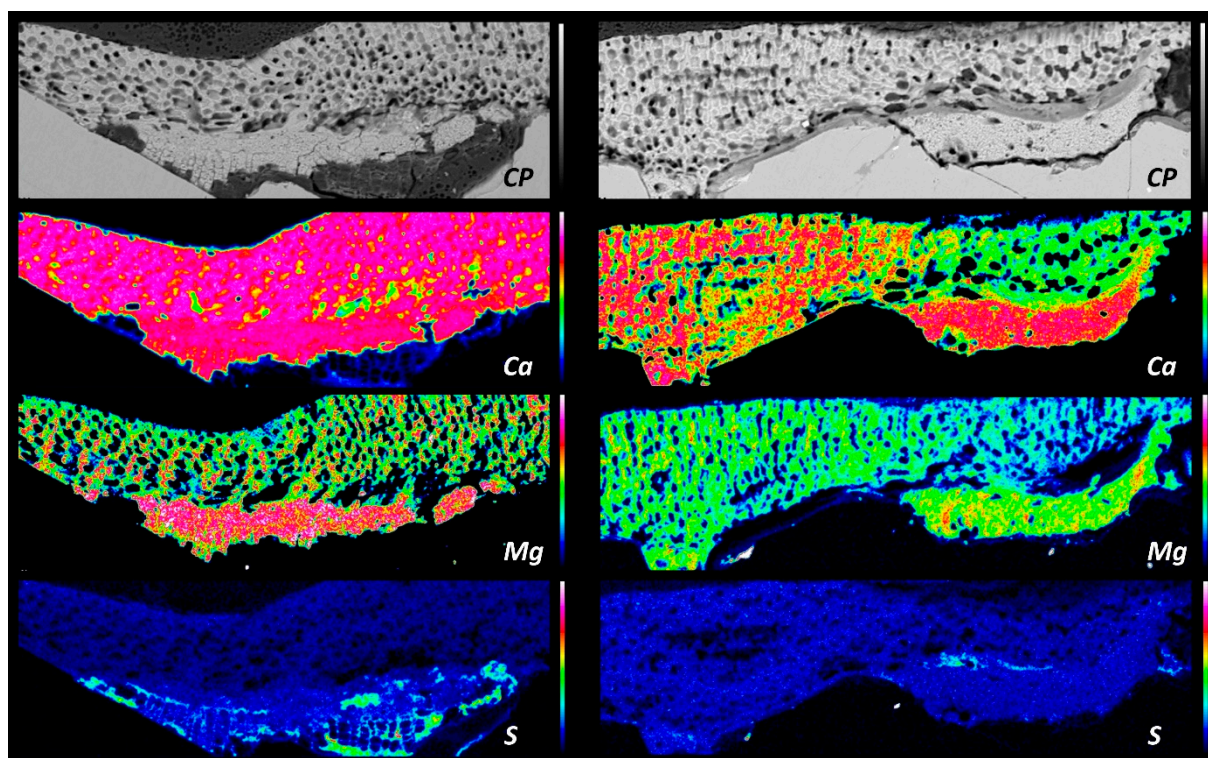
Figure 8. EMP-maps 1 (left) and 2 (right) detailing parts of the ontogenetic transect in *T. antarcticum*. Each image is showing a compound image (CP) similar to a BSE-image, as well as semiquantitative distribution maps for Ca, Mg and S. Sulfur is tied to the organic rich basal thallus part and enriched at the organic cell walls. Mg is tied to the high-Mg calcite of the cemented cell walls. Spatial resolution 1×1 μm, map dimensions 500×150 μm. Color scales (map 2/map 3): CP 500–1600 cps/450–1850 cps, Mg 0–120 cps/20–85 cps, Ca 500–825 cps/0–900 cps, S 0–100 cps/0–162 cps.
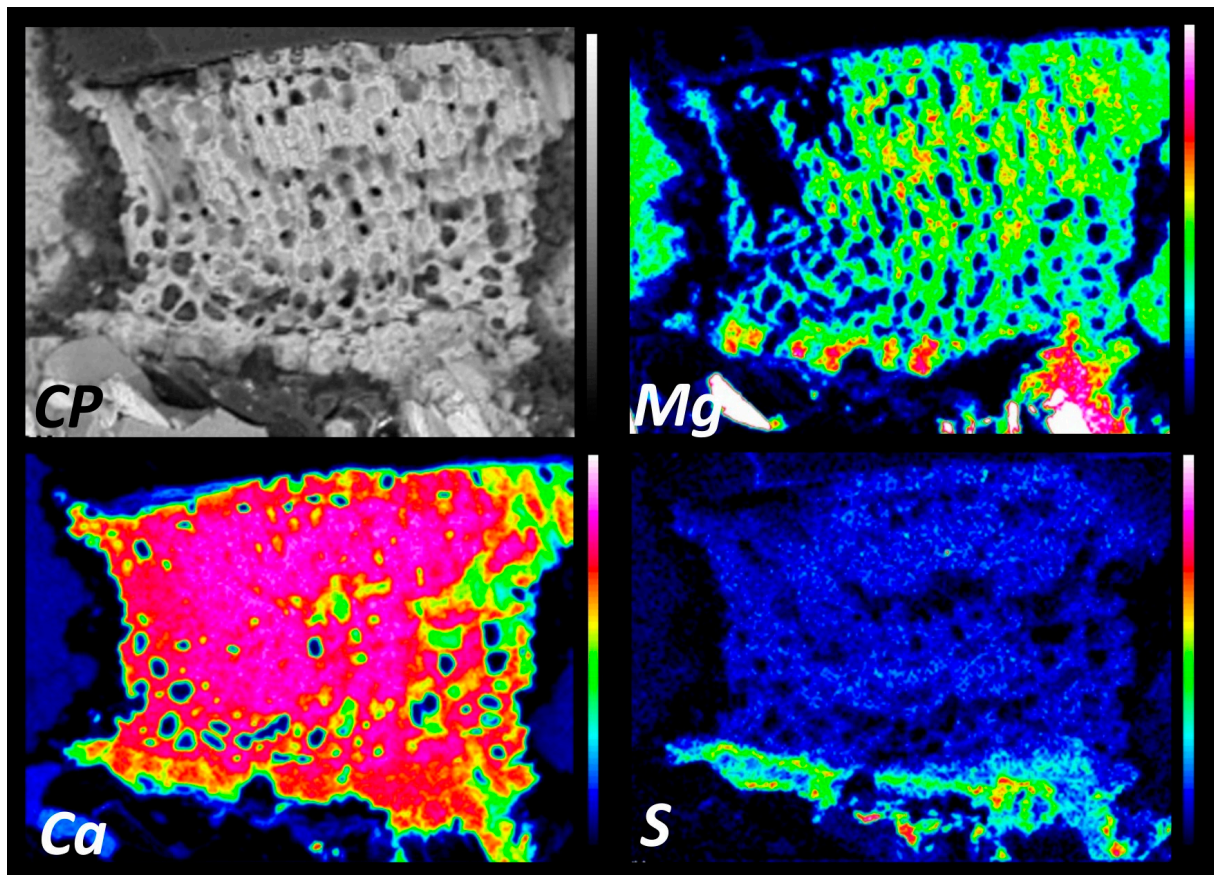
Figure 9. EMP-map 3, situated between two conceptacles. Sulfur is tied to the organic rich basal thallus part. Mg is tied to the high-Mg calcite of the cemented cell walls. Spatial resolution 1×1 μm, map dimensions 200×150 μm. Color scales: CP 1000–1500 cps, Mg 0–120 cps, Ca 0–900 cps, S 0–80 cps.

3.3. Elemental Maps

In all three areas mapped with the electron microprobe and visualized with BSE-imaging the same general vertical architecture of the thallus has been observed. In each, an organic-rich and poorly calcified layer forms the base in places where uneven topography of the polygonal crystalline bedrock was infilled. This non-calcified organic layer is characterized by box-shaped cells. Towards the contact with the main thallus, many cells were progressively filled with calcite and form a massive basal unit for the alga that accounts for its firm attachment. The main thallus layer above was characterized by a more porous lower zone with larger cells that are only partially calcified. These then curve upwards into parallel lines of equally sized cells that are oriented perpendicular to the upper thallus surface. These later cells are strongly calcified and show a fibrous Mg-calcite lining. This calcified zone shows a clearer crystal architecture than in the basal organic-rich stratum.

The organic-rich layer at the algal base is in all three mapping areas characterized by being rich in sulfur, while the main thallus has relatively low sulfur levels. S is spatially clearly tied to cell walls. Magnesium is absent from the purely organic portions and clearly tied to the calcitic portions of the basal layer. In fact, this zone appears slightly enriched in Mg with respect to the main thallus above. For the strongly calcified portion of the basal stratum and for the main thallus, the Ca contents showed no distinction. Sr and Mn had very low concentrations in the maps.

4. Discussion

The present study provides information on mineralogy and elemental composition of Ross Sea CCAs. This is important because, together with other high-Mg calcifiers [22,43] living in the polar regions, they will be the first responders to changes in temperature and seawater chemistry under predicted anthropogenic climate change scenarios.

The specimen description and taxonomy is largely in line with that from Sciuto et al. (2011) [19], however the cap of the multipore plates is not flat topped, as described by Sciuto, but it is dome shaped. The difference in morphology of samples collected in the same bay (Terra Nova Bay) and at the same depth, reinforce the need of molecular data to support the morpho-anatomical studies.

The sampling site in Terra Nova Bay is among the world´s coldest sites for CCA. The underwater observatory located at 25 m of depth in La Zecca, where algae were collected, recorded a full annual temperature cycle between November 2018 and November 2019. The temperature showed a minimum -1.95 °C in July 2019 and a maximim of $+1.08$ °C in November 2019 [23]. This 3 °C temperature fluctuation would be expected to result in an $MgCO_3$ variability of ~3 mol%, which corresponds well to the ± 1.57 mol% standard deviation around the average of 7.91 mol% $MgCO_3$ (Table 2). In fact, this lowest average $MgCO_3$ composition recorded for CCA is consistent with this coldest site temperature in the Ross Sea. At a global scale, the average site temperatures and average $MgCO_3$ compositions show overall a ~1 mol% shift per 1 °C [44,45] across the temperature span of ~3°C to ~30 °C, and our data integrate well with this trend. However, directly tying the minima and maxima of the full 6.5 mol% $MgCO_3$ range to the minimal and maximal temperatures recorded would result in a temperature proxy sensitivity about double of that recorded in other studies [44,45]. If the algal thallus grows year round and records all temperature conditions, would require confirmation by mark-recapture studies. Sea-ice prevails for most of the year in Terra Nova Bay and sea floor illumination is only recorded in austral summer between mid-January and April, with daily averages >20 E_V/lux [23]. Considering these short periods of sea ice free conditions, we consider it far more likely that the light-dependent thallus-growth reflects short and fast pulsed emplacement during austral summers. For a year-round growth under the extreme seasonality at the site, one would expect to see a clear $MgCO_3$ cyclicity, with winter troughs and summer highs, which is not the case in our ontogenetic EMP-transect (Figure 7, Table S2). This implies that the thallus-growth likely occurs in a temperature window between -0.5 to $+1.0$ °C. If this is correct, then the observed $MgCO_3$ average variability, as well as its full range, both exceed expected values. At these low annual temperature amplitudes of ~3 °C or even narrower summer temperature amplitudes of ~1.5 °C, the overriding influence of biological control on $MgCO_3$ during the mineralization of each architectural unit becomes visible. In theory, synchronously precipitated thallus parts experienced the same environmental conditions and should hence exhibit the same Mg-content. However, Fietzke et al. [46] observed a significant intra-increment variability for Mg/Ca via LA-ICP-MS mapping in *Clathromorphum nereostratum* and recommended replicate transects. Single ontogenetic tracks as for instance in, e.g., Hetzinger et al. [47,48] bear the risk to introduce unrecognized bias. Our single EMP-spot transect is hence a first insight to the composition of the Antarctic species *Tethysphytum antarcticum*. For a robust temperature calibration, marked-recaptured thalli with known growth duration are required, along with a replicate sampling within the same thallus and the thalli of further adjacent specimens. Moreover, it has been shown that the Mg/Ca ratio in CCA is not only impacted by temperature, but also by the available light as well as by pCO$_2$ [7,49,50].

Overall, $SrCO_3$ correlates with $MgCO_3$ ($MgCO_3 = 33.47 \times SrCO_3$; $r^2 = 0.89$) in our EMP-dataset, and both had been suggested as temperature proxies [49]. However, in the ontogenetic transect (Figure 7), the curves of $SrCO_3$ and $MgCO_3$ lack similarities, which again points to vital effects that outcompete temperature signals at the microscale [50].

A strict interpretation of Mg/Ca as a temperature proxy bears pitfalls for example through growth rate effects, which can influence B/Ca and also Mg/Ca in *Lithothamnium*

coralliodes [51]. In *T. antarcticum*, the single crustose thallus stratum consists of two layers visible in BSE-images and EMP maps (Figures 8 and 9) with clearly distinct geochemical compositions. In particular, average $MgCO_3$ with 11.78 ± 0.91 mol% is strongly increased in the basal layer, with respect to the main thallus layer above with 7.91 ± 1.57 mol%. Notwithstanding their contemporaneous emplacement, they differ in their $MgCO_3$ composition, but also in their sulphur content, with a strong enrichment of sulphur in the basal layers. In EMP-maps sulphur shows to be clearly enriched along the cell walls and is likely tied to the organic matrix. Continuity of the cell wall architecture from the basal thallus layer into the overlying main thallus layer stresses that they belong to the same specimen and do not represent the successive growth of two algal species. The basal layer smooths out the irregular substrate morphology and would need to be avoided during powder sampling for geochemistry. The bulk XRD analysis presented here derives from a zone without basal layer and the 8.04 mol% $MgCO_3$ calculated from the lattice parameters [43] overlaps with the overall average seen in quantitative EMP spot measurements. It should be noted here that the lattice parameters of the calcite are also affected by the $SrCO_3$ content, which probably leads to slight deviations in the actual $MgCO_3$ content from the value obtained from the calibration by Titschak et al. [43]. However, as the $SrCO_3$ contents are around factor 40 below the $MgCO_3$ contents (see Figure 7), this effect should be only minor. Interestingly, $SrCO_3$ does not show a distinction between the two layers and pairs of contemporaneously precipitated basal and main thallus overlap within instrumental error (Figure 7).

The basal layer of *T. antarcticum* is subsequently covered with very regular cells, that are arranged in filaments oriented perpendicular to the thallus and appear like a palisade in ontogenetic-longitudinal cross-sections. These contribute to the vertical gain in thickness of the thallus and appear layered in some parts. These possible layering does not show any difference in Mg content which is relatively constant along the thallus. Seasonal layering/bands with different Mg content are quite common in subpolar species such as *Clathomorphum nereostratum* and *Clathomorphum compactum* [7,52] or in free living coralline algae (rhodoliths) such as *Lithothamnnion glaciale* [6].

These increments with alternating lower and higher Mg contents correspond to different structures within the thallus with more calcified, smaller cells deposited in winter and larger, less calcified cells deposited in summer. Since, as previously stated, the Mg content is, amongst others such as light and CO_2 [50], driven by changes in water temperature, summer cells have a higher Mg content than the winter cells. It is possible that the seasonal temperature difference was not enough for making a substantial difference in Mg uptake by the algae.

Moreover, rhodolith and thick crust growth seems not to be hampered by a prolonged period of darkness and low temperature. Therefore, the lack of banding in *T. antarcticum* it is more likely to be related to the different growth pattern, rather than related to environmental variables [6,53]. *T. antarcticum* seems to grow mainly by marginal elongation and as such the lower growth rates in response to the predominantly marginal growth lead to a loss in resolution in the element variability along an ideal transect of the thickening as shown in the Mediterranean *Lithophyllum stictaeforme* [53].

5. Conclusions

DNA and molecular data, along with structural investigations clearly show an attribution of our sample to the newly described species *Tethysphytum antarcticum* Sciuto, Moschin & Moro, 2021. Our phylogenetic analyzes features the same issues as the one in Sciuto et al. [19], with a still unclear relation to members of the genus *Phymatolithon* Fosley, 1898. Our combined approach of thin section, SEM and μCT analyses revealed a hitherto undescribed basal layer in *T. antarcticum*. This layer is poorly calcified and organic-rich with box-shaped cells, which nevertheless attaches the alga firmly to its lithic substrate. This layer is rich in sulphur, which occurs tied to the organic cell walls. The mineralogy of the alga from XRD is clearly high-Mg calcite, yet with the relatively lowest measured

MgCO$_3$ concentration in all coralline algae. At global scale the Mg composition adheres to the temperature-dependent (amongst other factors such as pCO$_2$ and light) incorporation into the skeleton. At the local scale, with only 3 °C interannual temperature fluctuation, we see a higher Mg variability than expected, which highlights that further biological and environmental factors also impact the composition. We suggest a geochemical multi-proxy approach to further constrain intra-annual chemical variability. The establishment of time-series will require mark-recapture studies, optimally combined with the deployment of data loggers.

Supplementary Materials: The following are available online at https://www.mdpi.com/article/10.3390/min13020215/s1, Figure S1: Thin section images with translucent light (left) and polarized light under crossed-nichols (right), Figure S2: Raman spectra of two dominant minerals in the rock substrate beneath the algal crust are indicative of orthoclase (blue and purple) and phlogopite (red), Figure S3: Basic architecture of the calcareous coralline alga *Thetysphytum antarcticum* with conceptacles interspersed within the thallus (A), and a clear separation of a basal thallus and the main-thallus above (B), Table S1: Summarized unit cell parameters from Rietfeld refinement and MgCO$_3$ (mol%), Table S2: Quantitative EMP-spot measurements; XRD-machine parameters and raw data in TOPAS-format, as well as full spectra in text-file format are available under https://zenodo.org/record/7554165#.Y8p6hS9aZ-U.

References

1. Freiwald, A.; Henrich, R. Reefal Coralline Algal Build-Ups within the Arctic Circle: Morphology and Sedimentary Dynamics under Extreme Environmental Seasonality. *Sedimentology* **1994**, *41*, 963–984. [CrossRef]
2. Foster, M.S. Rhodoliths: Between Rocks and Soft Places. *J. Phycol.* **2001**, *37*, 659–667. [CrossRef]
3. Steller, D.L.; Riosmena-Rodríguez, R.; Foster, M.S.; Roberts, C.A. Rhodolith Bed Diversity in the Gulf of California: The Importance of Rhodolith Structure and Consequences of Disturbance. *Aquat. Conserv. Mar. Freshw. Ecosyst.* **2003**, *13*, S5–S20. [CrossRef]
4. Bilan, M.I.; Usov, A.I. Polysaccharides of Calcareous Algae and Their Effect on the Calcification Process. *Russ. J. Bioorgan. Chem.* **2001**, *27*, 2–16. [CrossRef]
5. Pavez, J.; Silva, J.F.; Melo, F. Effects of Alginic Acid from Marine Algae on Calcium Carbonate Electrodeposited Coating. *J. Cryst. Growth* **2005**, *282*, 438–447. [CrossRef]
6. Kamenos, N.A.; Cusack, M.; Moore, P.G. Coralline Algae Are Global Palaeothermometers with Bi-Weekly Resolution. *Geochim. Cosmochim. Acta* **2008**, *72*, 771–779. [CrossRef]

7. Williams, S.; Adey, W.; Halfar, J.; Kronz, A.; Gagnon, P.; Bélanger, D.; Nash, M. Effects of Light and Temperature on Mg Uptake, Growth, and Calcification in the Proxy Climate Archive *Clathromorphum Compactum*. *Biogeosciences* **2018**, *15*, 5745–5759. [CrossRef]
8. Chave, K.E. Aspects of the Biogeochemistry of Magnesium 1. Calcareous Marine Organisms. *J. Geol.* **1954**, *62*, 266–283. [CrossRef]
9. Ragazzola, F.; Kolzenburg, R.; Zekonyte, J.; Teichert, S.; Jiang, C.; Žuljević, A.; Caragnano, A.; Falace, A. Structural and Elemental Analysis of the Freshwater, Low-Mg Calcite Coralline Alga Pneophyllum Cetinaensis. *Plants* **2020**, *9*, 1089. [CrossRef]
10. De Carvalho, R.T.; Rocha, G.M.; Karez, C.S.; da Gama Bahia, R.; Pereira, R.C.; Bastos, A.C.; Salgado, L.T. Global Assessment of Coralline Algae Mineralogy Points to High Vulnerability of Southwestern Atlantic Reefs and Rhodolith Beds to Ocean Acidification. *Sci. Rep.* **2022**, *12*, 9589. [CrossRef]
11. Steneck, R.S. The Ecology of Coralline Algal Crusts: Convergent Patterns and Adaptative Strategies. *Annu. Rev. Ecol. Syst.* **1986**, *17*, 273–303. [CrossRef]
12. Zaneveld, J.S.; Sanford, R.B. Crustose Corallinaceous Algae (Rhodophyta) of the New Zealand and United States Scientific Expedition to the Ross Sea, Balleny Islands, and Macquarie Ridge, 1965. *Blumea Biodivers. Evol. Biogeogr. Plants* **1980**, *26*, 205–231.
13. Connell, S.D. The Monopolization of Understorey Habitat by Subtidal Encrusting Coralline Algae: A Test of the Combined Effects of Canopy-Mediated Light and Sedimentation. *Mar. Biol.* **2003**, *142*, 1065–1071. [CrossRef]
14. Schwarz, A.-M.; Hawes, I.; Andrew, N.; Mercer, S.; Cummings, V.; Thrush, S. Primary Production Potential of Non-Geniculate Coralline Algae at Cape Evans, Ross Sea, Antarctica. *Mar. Ecol. Prog. Ser.* **2005**, *294*, 131–140. [CrossRef]
15. Cinelli, F.; Mendoza, M.L.; Cabioch, J. Note Sur Quelques Espèces de Corallinacées (Rhodophyta) Recoltées Dans l'Antarctique. *Phycologia* **1989**, *28*, 136–139. [CrossRef]
16. Guiry, M.; Guiry AlgaeBase. World-Wide Electronic Publication. 2013. Available online: http://www.algaebase.org (accessed on 30 January 2023).
17. Foslie, M. Det Kongelige Norske Videnskabers Selskabs Aarsbertning. *Det. K. Nor. Vidensk. Selsk. Aarsbertning* **1904**, *6*, 15–18.
18. Miller, K.A.; Pearse, J.S. Ecological Studies of Seaweeds in McMurdo Sound, Antarctica. *Am. Zool.* **1991**, *31*, 35–48. [CrossRef]
19. Sciuto, K.; Moschin, E.; Alongi, G.; Cecchetto, M.; Schiaparelli, S.; Caragnano, A.; Rindi, F.; Moro, I. *Tethysphytum antarcticum* Gen. et Sp. Nov. (Hapalidiales, Rhodophyta), a New Non-Geniculate Coralline Alga from Terra Nova Bay (Ross Sea, Antarctica): Morpho-Anatomical Characterization and Molecular Phylogeny. *Eur. J. Phycol.* **2021**, *56*, 416–427. [CrossRef]
20. Pezzolesi, L.; Peña, V.; Le Gall, L.; Gabrielson, P.W.; Kaleb, S.; Hughey, J.R.; Rodondi, G.; Hernandez-Kantun, J.J.; Falace, A.; Basso, D.; et al. Mediterranean *Lithophyllum stictiforme* (Corallinales, Rhodophyta) Is a Genetically Diverse Species Complex: Implications for Species Circumscription, Biogeography and Conservation of Coralligenous Habitats. *J. Phycol.* **2019**, *55*, 473–492. [CrossRef]
21. Peña, V.; Hernandez-Kantun, J.J.; Adey, W.H.; Gall, L.L. Assessment of Coralline Species Diversity in the European Coasts Supported by Sequencing of Type Material: The Case Study of *Lithophyllum nitorum* (Corallinales, Rhodophyta). *Cryptogam. Algol.* **2018**, *39*, 123–137. [CrossRef]
22. Duquette, A.; Halanych, K.M.; Angus, R.A.; Mcclintock, J.B. Inter and Intraspecific Comparisons of the Skeletal Mg/Ca Ratios of High Latitude Antarctic Echinoderms. *Antarct. Sci.* **2018**, *30*, 160–169. [CrossRef]
23. Lombardi, C.; Kuklinski, P.; Bordone, A.; Spirandelli, E.; Raiteri, G. Assessment of Annual Physico-Chemical Variability via High-Temporal Resolution Monitoring in an Antarctic Shallow Coastal Site (Terra Nova Bay, Ross Sea). *Minerals* **2021**, *11*, 374. [CrossRef]
24. Deppeler, S.L.; Davidson, A.T. Southern Ocean Phytoplankton in a Changing Climate. *Front. Mar. Sci.* **2017**, *4*, 40. [CrossRef]
25. Sabine, C.L.; Feely, R.A.; Gruber, N.; Key, R.M.; Lee, K.; Bullister, J.L.; Wanninkhof, R.; Wong, C.S.; Wallace, D.W.R.; Tilbrook, B.; et al. The Oceanic Sink for Anthropogenic CO_2. *Science* **2004**, *305*, 367–371. [CrossRef]
26. Barnes, D.K.A. Polar zoobenthos blue carbon storage increases with sea ice losses, because across-shelf growth gains from longer algal blooms outweigh ice scour mortality in the shallows. *Glob. Chang. Biol.* **2017**, *23*, 5083–5091. [CrossRef]
27. Gutt, J.; Isla, E.; Bertler, A.N.; Bodeker, G.E.; Bracegirdle, T.J.; Cavanagh, R.D.; Comiso, J.C.; Convey, P.; Cummings, V.; De Conto, R.; et al. Cross-disciplinarity in the advance of Antarctic ecosystem research. *Mar. Gen.* **2017**, *37*, 1–17. [CrossRef]
28. Henley, S.F.; Schofield, O.M.; Hendry, K.R.; Schloss, I.R.; Steinberg, D.K.; Moffat, C.; Peck, L.S.; Costa, D.P.; Bakker, D.C.; Hughes, C.; et al. Variability and change in the west Antarctic Peninsula marine system: Research priorities and opportunities. *Prog. Oceanogr.* **2019**, *173*, 208–237.
29. Illuminati, S.; Annibaldi, A.; Romagnoli, T.; Libani, G.; Antonucci, M.; Scarponi, G.; Totti, C.; Truzzi, C. Distribution of Cd, Pb and Cu between dissolved fraction, inorganic particulate and phytoplankton in seawater of Terra Nova Bay (Ross Sea, Antarctica) during austral summer 2011–12. *Chemosphere* **2017**, *185*, 1122–1135. [CrossRef]
30. Budillon, G.; Pacciaroni, M.; Cozzi, S.; Rivaro, P.; Catalano, G.; Ianni, C.; Cantoni, C. An optimum multiparameter mixing analysis of the shelf waters in the Ross Sea. *Antarct. Sci.* **2003**, *15*, 105–118. [CrossRef]
31. Nihashi, S.; Ohshima, K.I. Circumpolar Mapping of Antarctic Coastal Polynyas and Landfast Sea Ice: Relationship and Variability. *J. Clim.* **2015**, *28*, 3650–3670. [CrossRef]
32. Faranda, F.M.; Guglielmo, L.; Ianora, A. The Italian oceanographic cruises in the Ross Sea (1987–1995): Strategy, general consideration description of the sampling sites. In *Ross Sea Ecology*; Faranda, F.M., Guglielmo, L., Ianora, A., Eds.; Springer: Berlin/Heidelberg, Germany, 2000; pp. 1–14.
33. Pusceddu, A.; Dell'Anno, A.; Fabiano, M. Organic matter composition in coastal sediments at Terra Nova Bay (Ross Sea) during summer 1995. *Polar Biol.* **2000**, *23*, 288–293. [CrossRef]

34. Silvano, A.; Foppert, A.; Rintoul, S.R.; Holland, P.R.; Tamura, T.; Kimura, N.; Castagno, P.; Falco, P.; Budillon, G.; Haumann, F.A.; et al. Recent recovery of Antarctic BottomWater formation in the Ross Sea driven by climate anomalies. *Nat. Geosci.* **2020**, *13*, 780–786. [CrossRef]
35. Caputi, S.S.; Careddu, G.; Calizza, E.; Fiorentino, F.; Maccapan, D.; Rossi, L.; Costantini, M.L. Seasonal Food Web Dynamics in the Antarctic Benthos of Tethys Bay (Ross Sea): Implications for Biodiversity Persistence Under Different Seasonal Sea-Ice Coverage. *Front. Mar. Sci.* **2020**, *7*, 594454. [CrossRef]
36. Calizza, E.; Rossi, L.; Careddu, G.; Caputi, S.S.; Costantini, M.L. Species richness and vulnerability to disturbance propagation in real food webs. *Sci. Rep.* **2019**, *9*, 19331. [CrossRef] [PubMed]
37. Clark, G.F.; Stark, J.S.; Palmer, A.S.; Riddle, M.J.; Johnston, E.L. The Roles of Sea-Ice, Light and Sedimentation in Structuring Shallow Antarctic Benthic Communities. *PLoS ONE* **2017**, *12*, e0168391. [CrossRef] [PubMed]
38. Pearse, J.S.; McClintock, J.B.; Bosch, I. Reproduction of Antarctic Benthic Marine Invertebrates: Tempos, Modes, and Timing. *Am. Zoöl.* **1991**, *31*, 65–80. [CrossRef]
39. Yoon, H.S.; Hackett, J.D.; Bhattacharya, D. A Single Origin of the Peridinin- and Fucoxanthin-Containing Plastids in Dinoflagellates through Tertiary Endosymbiosis. *Proc. Natl. Acad. Sci. USA* **2002**, *99*, 11724–11729. [CrossRef]
40. Maneveldt, G.W.; Jeong, S.Y.; Cho, T.O.; Hughey, J.R.; Gabrielson, P.W. Reassessment of Misapplied Names, Phymatolithon Ferox and P. Repandum (Hapalidiales, Corallinophycidae, Rhodophyta) in South Africa, Based on DNA Sequencing of Type and Recently Collected Material. *Phycologia* **2020**, *59*, 449–455. [CrossRef]
41. Kumar, S.; Stecher, G.; Li, M.; Knyaz, C.; Tamura, K. MEGA X: Molecular Evolutionary Genetics Analysis across Computing Platforms. *Mol. Biol. Evol.* **2018**, *35*, 1547–1549. [CrossRef]
42. Di Vincenzo, G.; Rocchi, S. Origin and interaction of mafic and felsic magmas in an evolving late orogenic setting: The Early Paleozoic Terra Nova Intrusive Complex, Antarctica. *Contrib. Mineral. Petrol.* **1999**, *137*, 15–35. [CrossRef]
43. Titschack, J.; Goetz-Neunhoeffer, F.; Neubauer, J. Magnesium Quantification in Calcites [(Ca,Mg)CO3] by Rietveld-Based XRD Analysis: Revisiting a Well-Established Method. *Am. Mineral.* **2011**, *96*, 1028–1038. [CrossRef]
44. Henrich, R.; Freiwald, A.; Wehrmann, A.; Schäfer, P.; Samtleben, C.; Zankl, H. Nordic cold-water carbonates: Occurrences and controls. In *Global and Regional Controls on Biogenic Sedimentation, I: Reef Evolution. Research Reports*; Göttinger Arbeiten zur Geologie und Paläontologie: Göttingen, Germany, 1996.
45. Halfar, J.; Zack, T.; Kronz, A.; Zachos, J.C. Growth and High-Resolution Paleoenvironmental Signals of Rhodoliths (Coralline Red Algae): A New Biogenic Archive. *J. Geophys. Res. Oceans* **2000**, *105*, 22107–22116. [CrossRef]
46. Fietzke, J.; Ragazzola, F.; Halfar, J.; Dietze, H.; Foster, L.C.; Hansteen, T.H.; Eisenhauer, A.; Steneck, R.S. Century-Scale Trends and Seasonality in PH and Temperature for Shallow Zones of the Bering Sea. *Proc. Natl. Acad. Sci. USA* **2015**, *112*, 2960–2965. [CrossRef] [PubMed]
47. Hetzinger, S.; Halfar, J.; Kronz, A.; Steneck, R.S.; Adey, W.; Lebednik, P.A.; Schöne, B.R. High-Resolution Mg/Ca Ratios in a Coralline Red Alga as a Proxy for Bering Sea Temperature Variations from 1902 to 1967. *Palaios* **2009**, *24*, 406–412. [CrossRef]
48. Hetzinger, S.; Halfar, J.; Zack, T.; Gamboa, G.; Jacob, D.E.; Kunz, B.E.; Kronz, A.; Adey, W.; Lebednik, P.A.; Steneck, R.S. High-Resolution Analysis of Trace Elements in Crustose Coralline Algae from the North Atlantic and North Pacific by Laser Ablation ICP-MS. *Palaeogeogr. Palaeoclimatol. Palaeoecol.* **2011**, *302*, 81–94. [CrossRef]
49. Kamenos, N.A.; Hoey, T.B.; Nienow, P.; Fallick, A.E.; Claverie, T. Reconstructing Greenland Ice Sheet Runoff Using Coralline Algae. *Geology* **2012**, *40*, 1095–1098. [CrossRef]
50. Teichert, S.; Voigt, N.; Wisshak, M. Correction to: Do Skeletal Mg/Ca Ratios of Arctic Rhodoliths Reflect Atmospheric CO2 Concentrations? *Polar Biol.* **2021**, *44*, 1745. [CrossRef]
51. Piazza, G.; Bracchi, V.A.; Langone, A.; Meroni, A.N.; Basso, D. Growth Rate Rather than Temperature Affects the B/Ca Ratio in the Calcareous Red Alga *Lithothamnion corallioides*. *Biogeosciences* **2022**, *19*, 1047–1065. [CrossRef]
52. Gould, J.; Halfar, J.; Adey, W.; Ries, J.B. Growth as a Function of Sea Ice Cover, Light and Temperature in the Arctic/Subarctic Coralline C. Compactum: A Year-Long in Situ Experiment in the High Arctic. *Front. Mar. Sci.* **2022**, *9*, 900033. [CrossRef]
53. Ragazzola, F.; Caragnano, A.; Basso, D.; Schmidt, D.N.; Fietzke, J. Establishing Temperate Crustose Early Holocene Coralline Algae as Archives for Palaeoenvironmental Reconstructions of the Shallow Water Habitats of the Mediterranean Sea. *Palaeontology* **2020**, *63*, 155–170. [CrossRef]